## Supporting Information

Here are provided twelve supplementary figures and one supplementary table. The first three figures demonstrate the quality of the fit for the simultaneous target analysis of eight datasets as reported in the main text and show the residual analysis. The next four figures show the full kinetic scheme used in the target analysis of the different samples for both S1 and S2. Then a figure showing the reconstructed decay associated spectra (DAS) from the target analysis as well complete table with corresponding lifetimes and assignments of these lifetimes to the different subunits of the target model. Finally the complete target analysis of the data on the chemically locked S1 to S2 transition reported in (Wlodarczyk et al. 2015) with the target model from this work (and analogous figures).

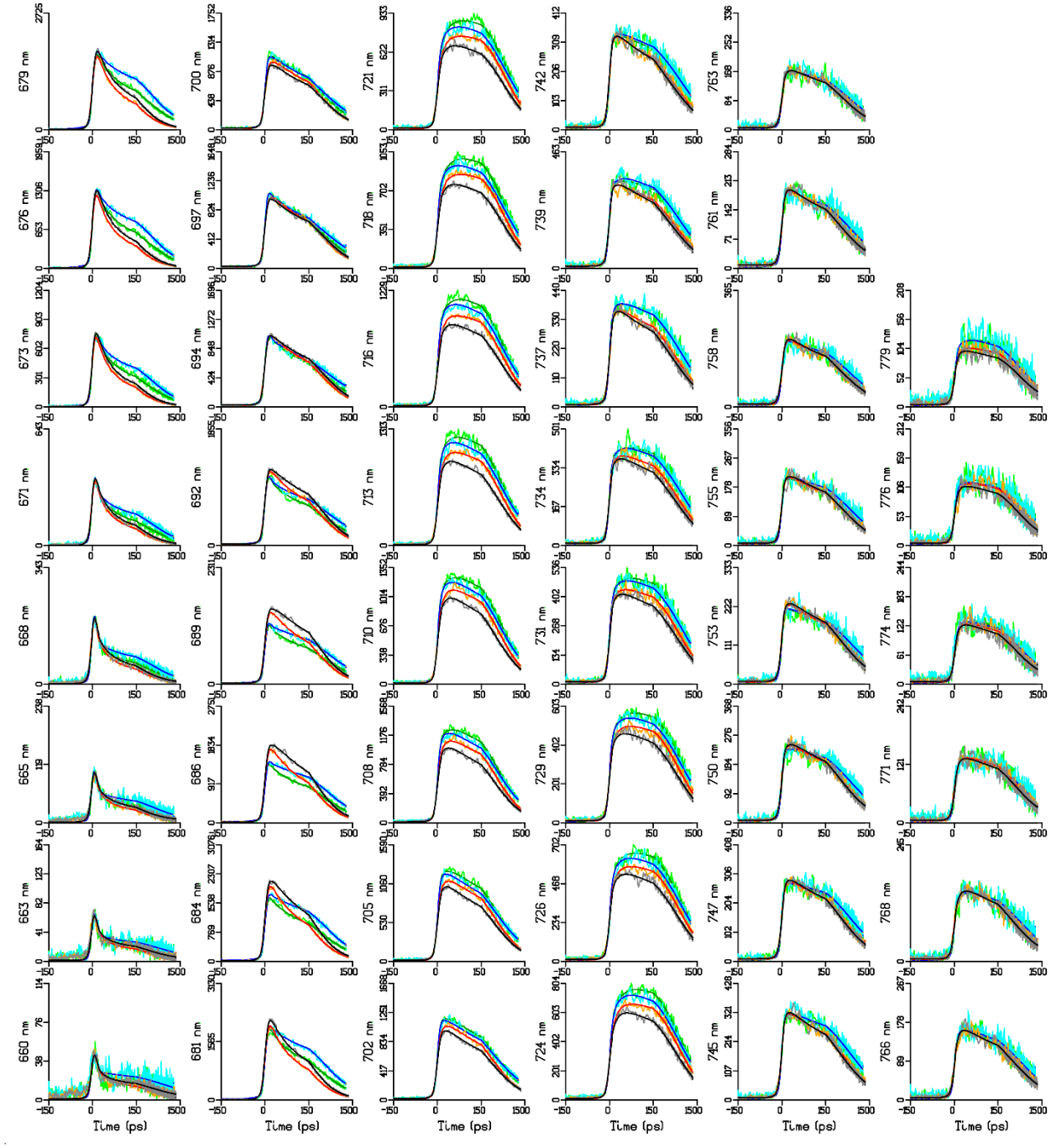


Figure S 1: Time-resolved emission (traces scaled to their maximum) at 46 wavelengths (indicated in the ordinate label) after excitation with 400 nm. Data for WT S1 & S2 shown in gray and orange, black and red lines indicate the fit after target analysis. Data for FUD7 S1 & S2 shown in cyan and light green, fit in blue and dark green respectively. Note that the time axis is linear until 150 ps, and logarithmic thereafter.

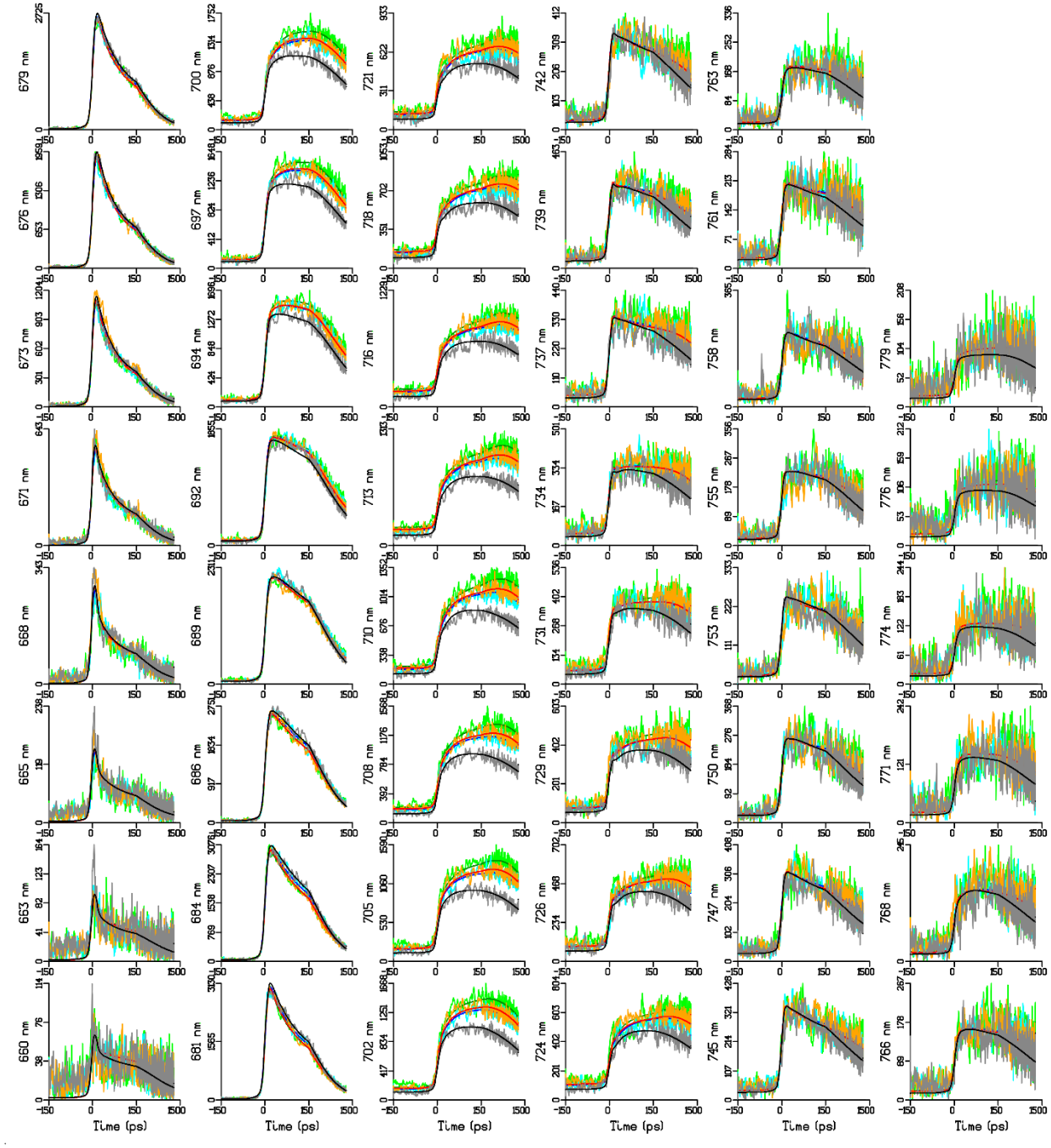


Figure S 2. Time-resolved emission (traces scaled to their maximum) at 46 wavelengths (indicated in the ordinate label) after excitation with 400 nm. Data for F15 S1 & S2 shown in gray and orange, black and red lines indicate the fit after target analysis. Data for M18 S1 & S2 shown in cyan and light green, fit in blue and dark green respectively. Note that the time axis is linear until 150 ps, and logarithmic thereafter.

In addition to visually inspecting the individual traces, it is also necessary to do a singular value decomposition (SVD) of the residual matrix to reveal possible significant structure in the residual matrix. For each of the four pairs of datasets, WT, FUD7, F15 and M18 in State 1 and State 2 the first left and right singular vector of the SVD are depicted in Figure S 3. We observe no systematic trends that would warrant adding components to the model.

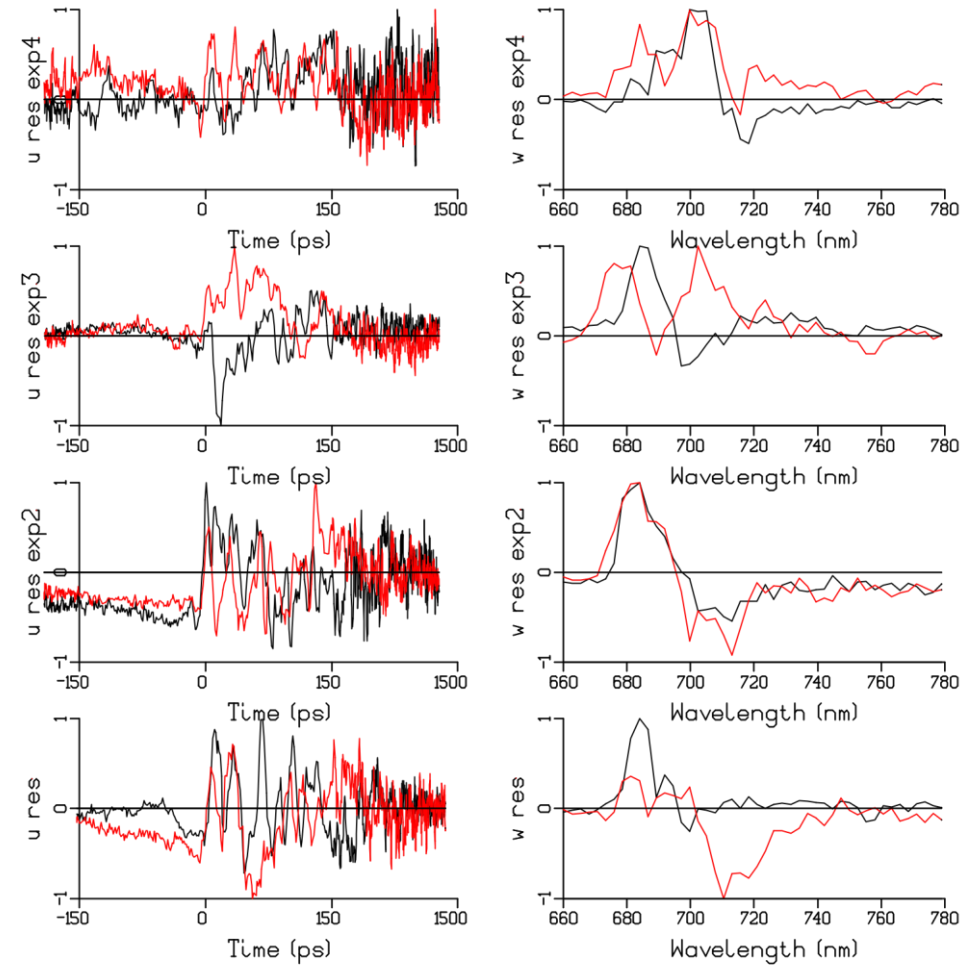


Figure S 3.The first left (u res) and right (w res) singular vectors resulting from a singular value decomposition of the residual matrix for the 8 simultaneously analyzed datasets. S1 is depicted in black, S2 in red. From bottom to top are shown WT, FUD7, F15 and M18. Note that the time axis is linear until 150 ps, and logarithmic thereafter.

***Full kinetic schemes for each sample in the simultaneous analysis of all eight datasets.***

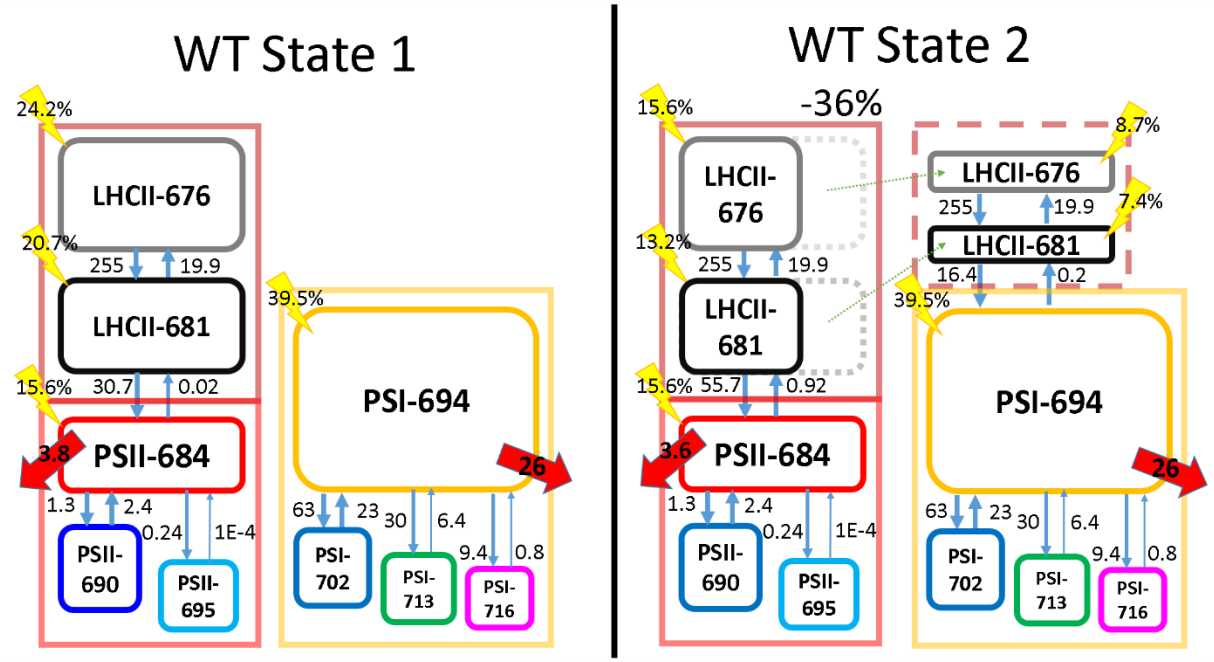


Figure S 4. Full kinetic scheme used in the target analysis of the WT datasets in S1 and S2. Here we combine the compartmental schemes from Figure 2 and Figure 4 with the information from Table 1, thus providing a detailed view of Figure 6. The relative input in each compartment is given as percentage of the total, all rates are given in /ns. The dashed green arrows in State 2 indicate the state transition, and the relative amount of LHCII involved (36%) is written on top.

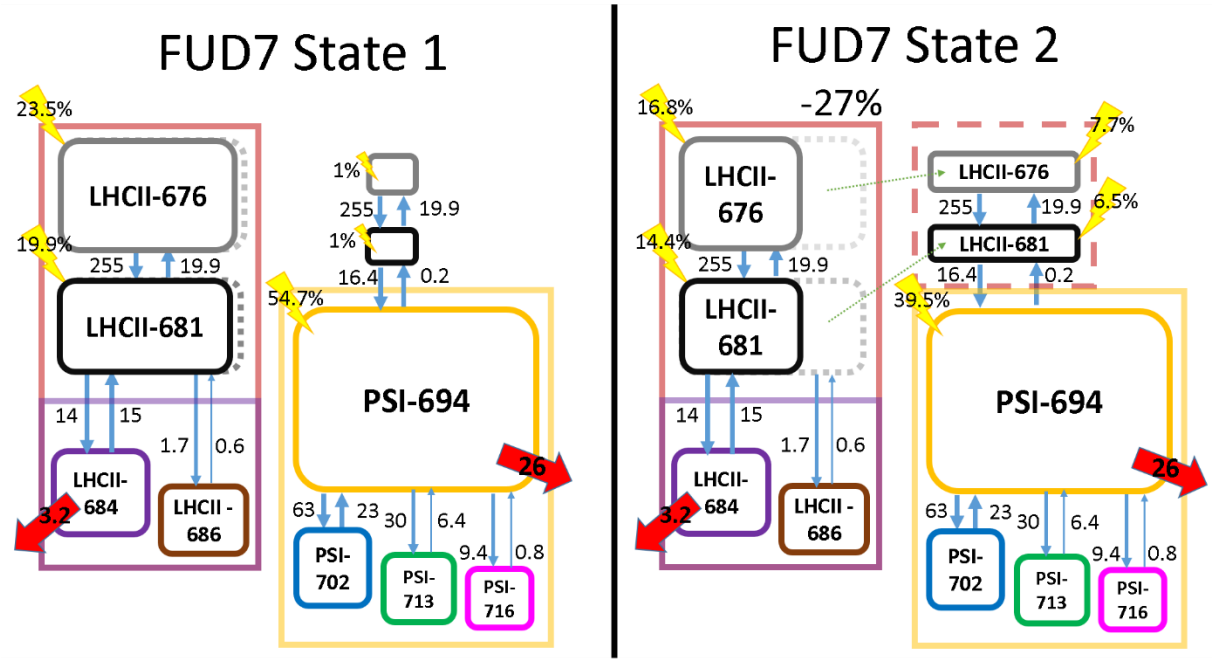


Figure S 5. Full kinetic scheme used in the target analysis of the FUD7 datasets in S1 and S2. Here we combine the compartmental schemes from Figure 3 and Figure 4 with the information from Table 1. Further information, see the caption of Figure S 4.

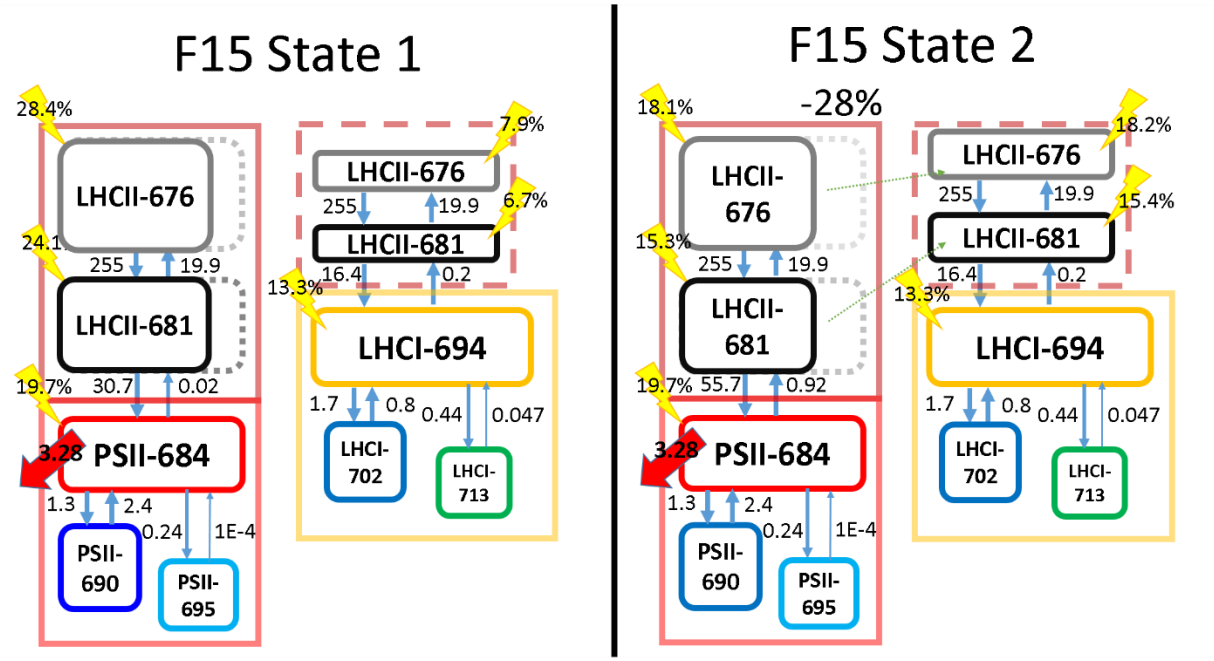


Figure S 6. Full kinetic scheme used in the target analysis of the F15 datasets in S1 and S2. Here we combine the compartmental schemes from Figure 2 and Figure 5 with the information from Table 1. Further information, see the caption of Figure S 4.

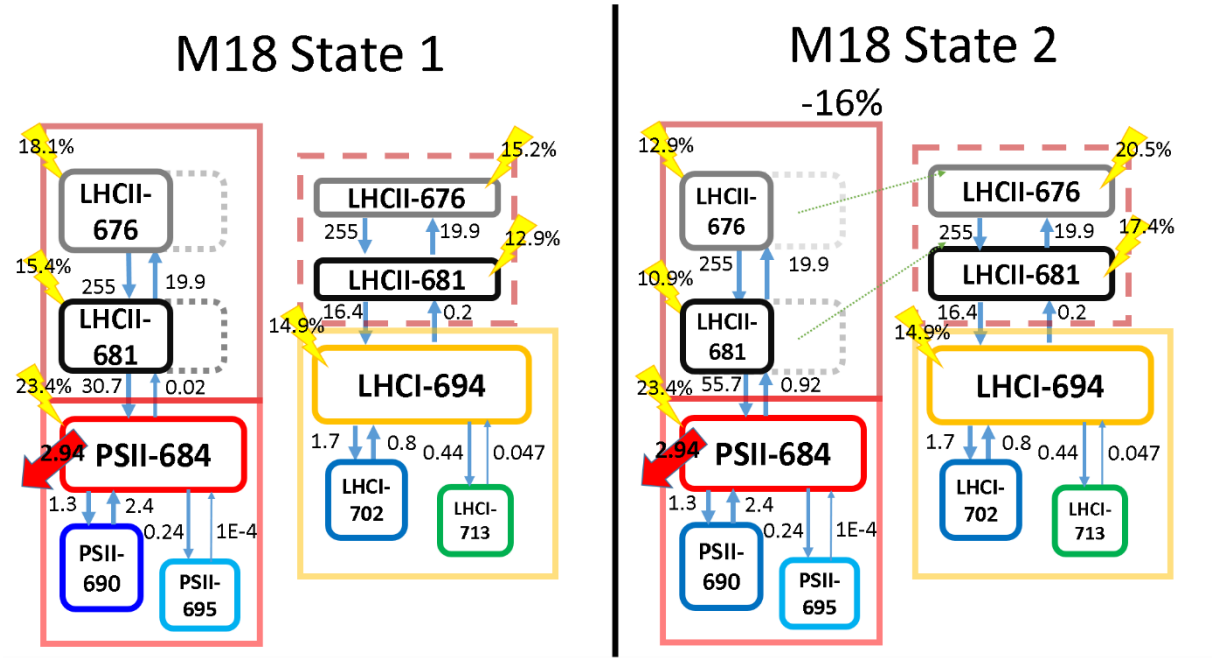


Figure S 7. Full kinetic scheme used in the target analysis of the M18 datasets in S1 and S2. Here we combine the compartmental schemes from Figure 2 and Figure 5 with the information from Table 1. Further information, see the caption of Figure S 4.

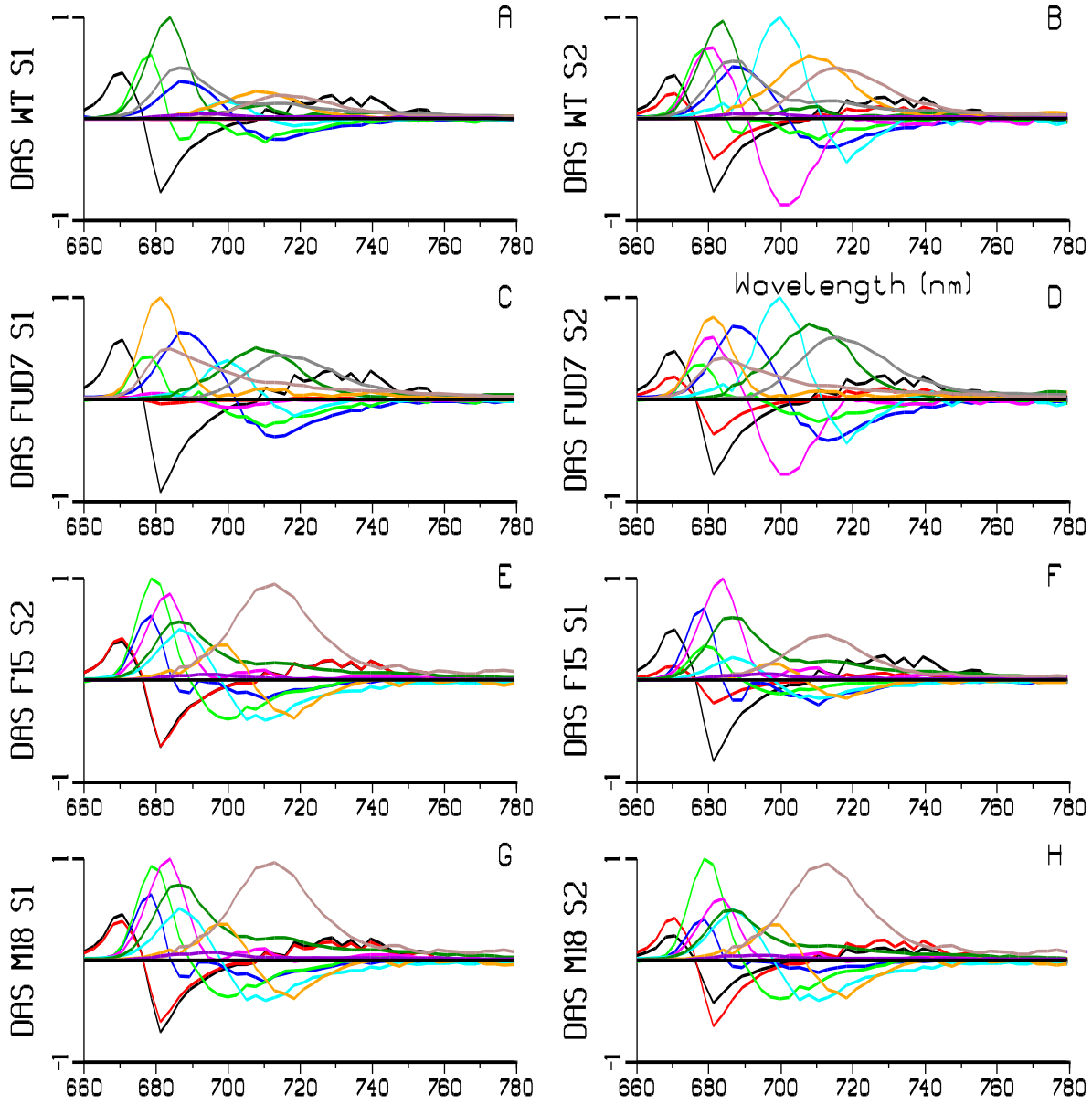


Figure S 8 Reconstructed DAS from the target analysis. Color key and lifetimes (in ps) indicated in Table S 1.

Table S 1. Lifetimes in picoseconds of the DAS of Figure S 8, with samples and their composition indicated.

| | τ1 | τ2 | τ3 | τ4 | τ5 | τ6 | τ7 | τ8 | τ9 | τ10 | τ11 | sample composition | |
|---|---|---|---|---|---|---|---|---|---|---|---|---|---|
| | Black | Red | Blue | Green | Magenta | Cyan | Darkgr | Orange | Grey | Brown | Purple | | |
| WT S1 | 3.61 | 3.62 | 7.0 | 35.2 | 64.8 | 75.8 | 161 | 303 | 576 | 1155 | 4998 | LHCII-LHCI-PSI | LHCII-PSII |
| WT S2 | 3.57 | 3.62 | 7.0 | 19.3 | 64.8 | 75.8 | 168 | 303 | 590 | 1155 | 4998 | LHCII-LHCI-PSI | LHCII-PSII |
| FUD7 S1 | 3.62 | 3.62 | 7.0 | 32.2 | 64.8 | 75.8 | 303 | 374 | 1155 | 2087 | | LHCII-LHCI-PSI | LHCII+ |
| FUD7 S2 | 3.62 | 3.62 | 7.0 | 32.2 | 64.8 | 75.8 | 303 | 374 | 1155 | 2087 | | LHCII-LHCI-PSI | LHCII+ |
| F15 S1 | 3.61 | 3.62 | 35.2 | 64.1 | 173 | 308 | 615 | 2049 | 3126 | 3128 | 4998 | LHCII-LHCI | LHCII-PSII |
| F15 S2 | 3.57 | 3.62 | 19.3 | 64.1 | 175 | 308 | 617 | 2049 | 3126 | 3128 | 4998 | LHCII-LHCI | LHCII-PSII |
| M18 S1 | 3.61 | 3.62 | 35.2 | 64.1 | 181 | 308 | 649 | 2049 | 3126 | 3128 | 4998 | LHCII-LHCI | LHCII-PSII |
| M18 S2 | 3.57 | 3.62 | 19.3 | 64.1 | 183 | 308 | 652 | 2049 | 3126 | 3128 | 4998 | LHCII-LHCI | LHCII-PSII |

## Target analysis of the chemically locked S1 to S2 transition from (Wlodarczyk et al. 2015)

*Chlamydomonas reinhardtii* wild-type (WT) which came from the lab of Prof. Jean-David Rochaix was used. The growth conditions, treatments and measurement protocols have been described in more detail before (Wlodarczyk et al. 2015). Briefly, the cells were grown under constant illumination with 25 μmol photons $m^{-2}$ $s^{-1}$ PAR in Tris-acetate-phosphate (TAP) medium at 25℃ with constant mixing (170 rpm) on an incubator shaker (Minitron, INFORS HT). Cells for measurements were harvested in a mid-logarithmic phase of growth ($OD_{750}$ ≈0.7). A batch of cells was then prepared in S1 by strongly aerating them in the dark for 90 min in the presence of 0.1 μM staurosporine, a kinase inhibitor which prevents phosphorylation of LHCII (Takahashi et al. 2006). This chemically locked state 1 was denoted as **S1c**. For state 2, cells were incubated 45 min under anaerobic conditions in the dark in the presence of sodium fluoride (0.1 M) in order to inhibit dephosphorylation of LHCII (Takahashi et al. 2006). This chemically locked state 2 was denoted as **S2c**. After induction of S1 or S2, intact *C.r.* cells were instantly frozen in the presence of glycerol as cryoprotectant (65% v/v) in nitrogen cryostat (Oxford) and kept in this state for the duration of the measurement. The samples were measured on a synchroscan streak-camera setup described in detail elsewhere (van Stokkum et al. 2006; van Stokkum et al. 2008). The excitation pulses (**475** nm, ≈100 fs) carried an energy per pulse of 14 nJ and were used to excite the sample with a repetition rate of 50 kHz. The resulting laser beam was focused on the sample giving a spot of ≈150 μm in diameter. Time-resolved emission in the window of 660 nm to 818 nm over a range of 1.5 ns with 1.5 ps step size was used for data analysis. The FWHM of the instrument response function (IRF) was found to be 14 ps. The time-resolved fluorescence of S1c and S2c were simultaneously analyzed with the same target model as presented in the main text.

For these data we present in Figure S 9 and Figure S 10 the compartmental model, concentration profiles and estimated SAS for respectively the LHCII-PSII and LHCII-LHCI-PSI supercomplex, analogous to Figure 2 and Figure 4 in the main text. In both figures the population profiles and the SAS from the main text have been added in panels D and E to facilitate visual comparison. The raw data traces overlaid with the fit shown in Figure S 11 show the satisfactory agreement of the present model with these data. However, a careful analysis of the residual matrix presented in Figure S 12 analogous to Figure S 3 does reveal a significant residual concentrated around 685 nm. This is what in the previous paper (Wlodarczyk et al. 2015) was captured by a component designated X-685 and which is now missing from the used target model because it was not necessary to fit the data reported on in the main text. Apparently, X-685 is only present after a “chemically induced” state transition. Note that the “chemically induced” state transition is larger than the “nonchemically induced” state transition, compare the relative differences between the solid and dashed lines in Figure S 9B and D and in Figure S 10B and D. This can only partly be attributed to the 475 instead of 400 nm excitation.

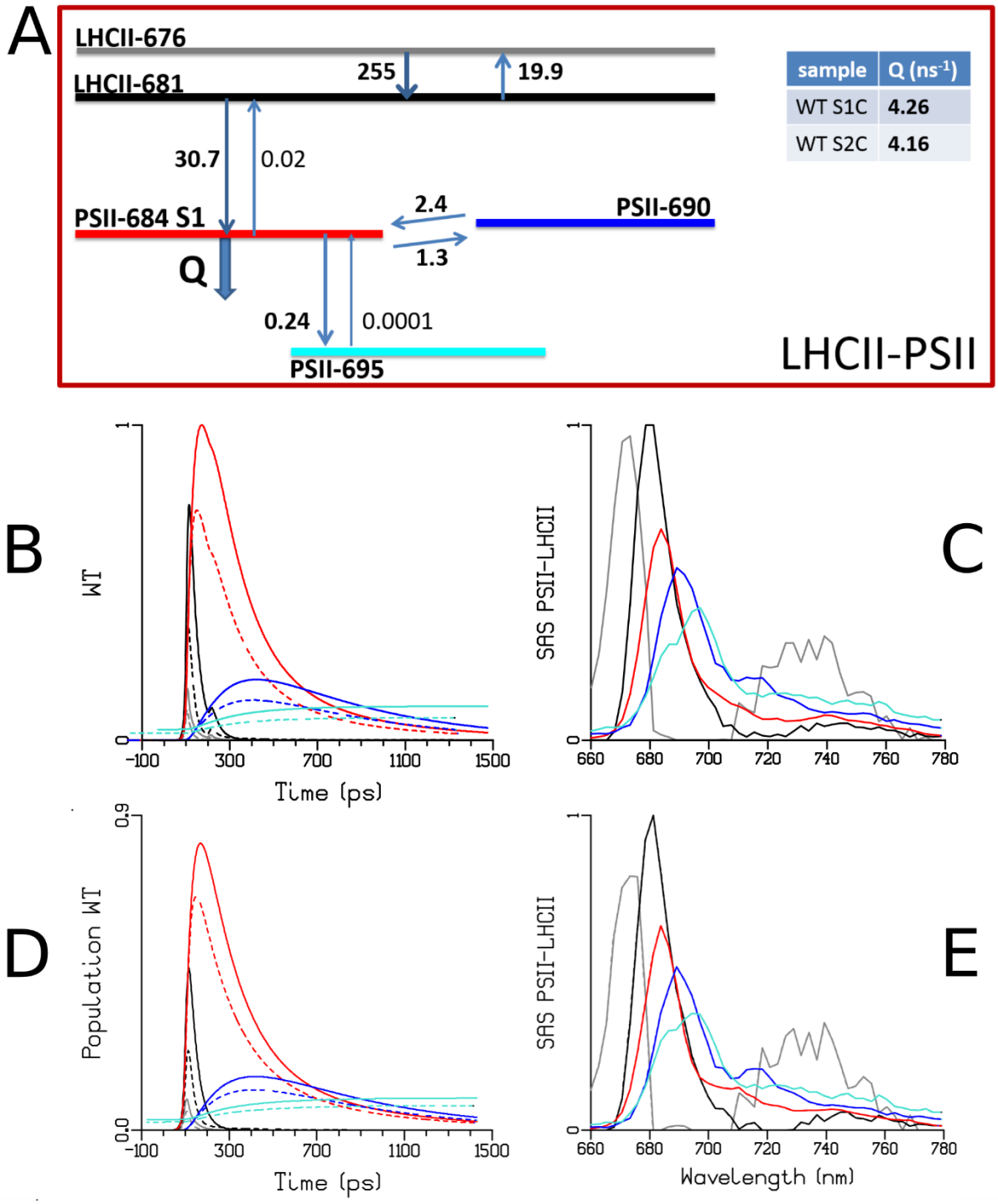


Figure S 9. Compartmental model for the LHCII-PSII supercomplex at 77 K. All rates are in $ns^{-1}$ and fixed to the estimated values reported in the main text, except for the variable quenching rate Q which remained a free parameter (inset table). B) Population dynamics in WT (S1c solid, S2c dashed) and C) estimated SAS for the **S1c** and **S2c** data. D) Population dynamics in WT (S1 solid, S2 dashed) and E) estimated SAS for the **S1** and **S2** data.

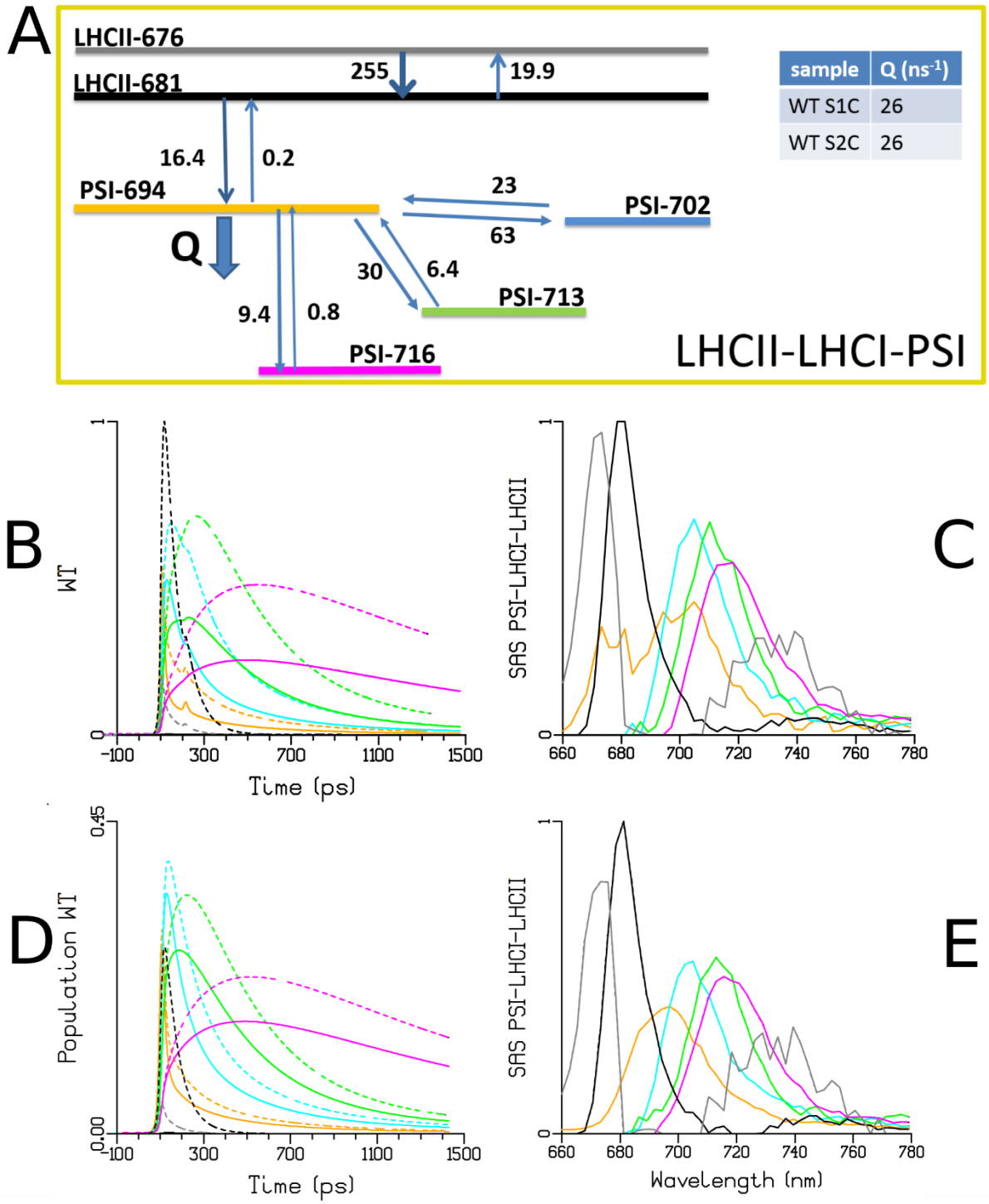


Figure S 10. A) Compartmental model for the LHCII-LHCI-PSI subunit at 77K. All rates are in $ns^{-1}$ and fixed to the estimated values reported in the main text. B) Population dynamics in WT (S1c solid, S2c dashed) and C) estimated SAS for the **S1c** and **S2c** data. D) Population dynamics in WT (S1 solid, S2 dashed) and E) estimated SAS for the **S1** and **S2** data.

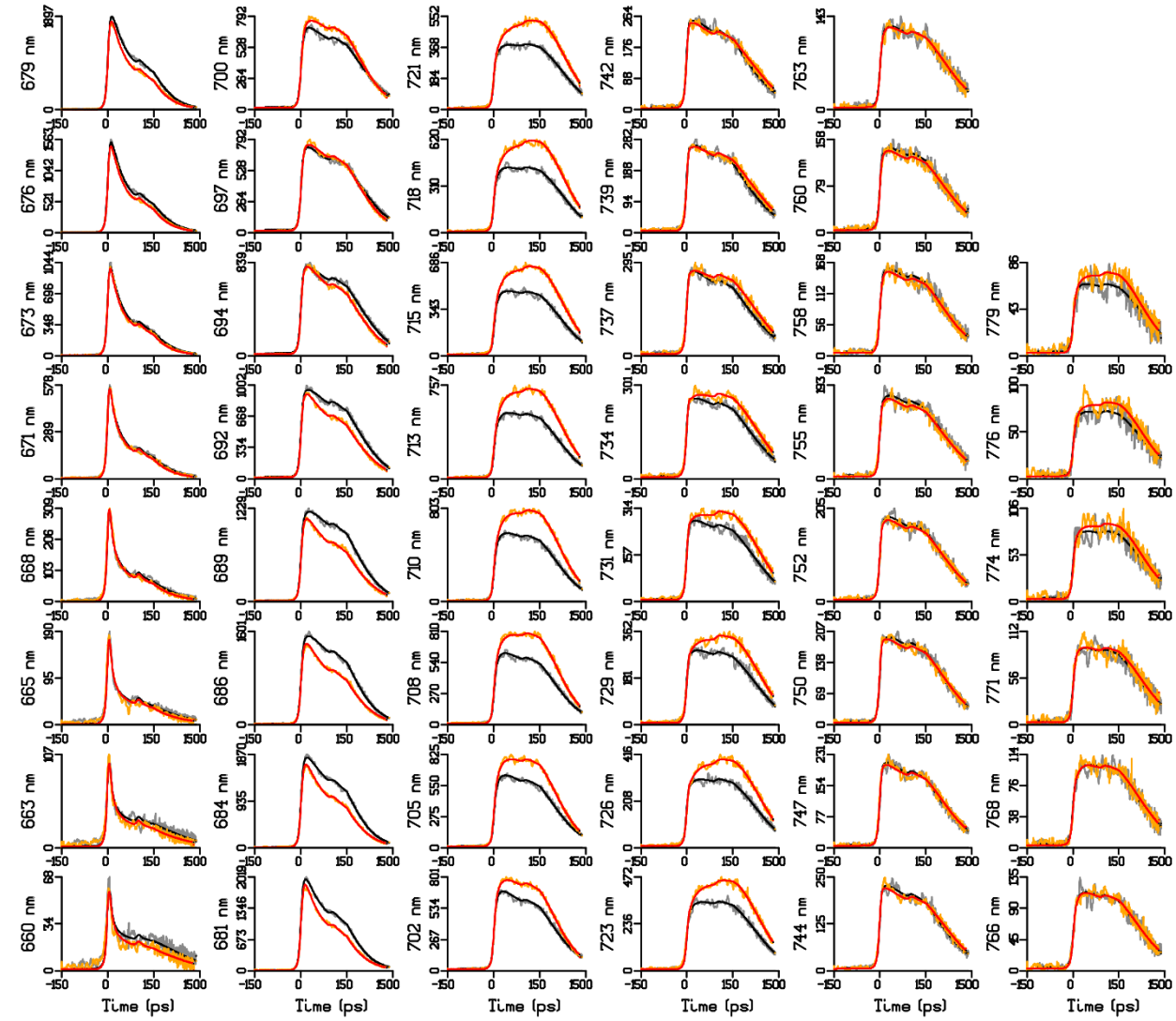


Figure S 11. Time-resolved emission (traces scaled to their maximum) at 46 wavelengths (indicated in the ordinate label) after 475 nm excitation of intact, instantly frozen C.r. cells poised in S1 or in S2 (chemically locked) as described in (Wlodarczyk et al. 2015); see also Figure S3 and Figure S4 of that reference. In gray and orange is shown the data for WT S1c & S2c, black and red lines indicate the fit after target analysis using the model reported in this paper (see Figure S 9, Figure S 10). Note that the time axis is linear until 150 ps, and logarithmic thereafter.

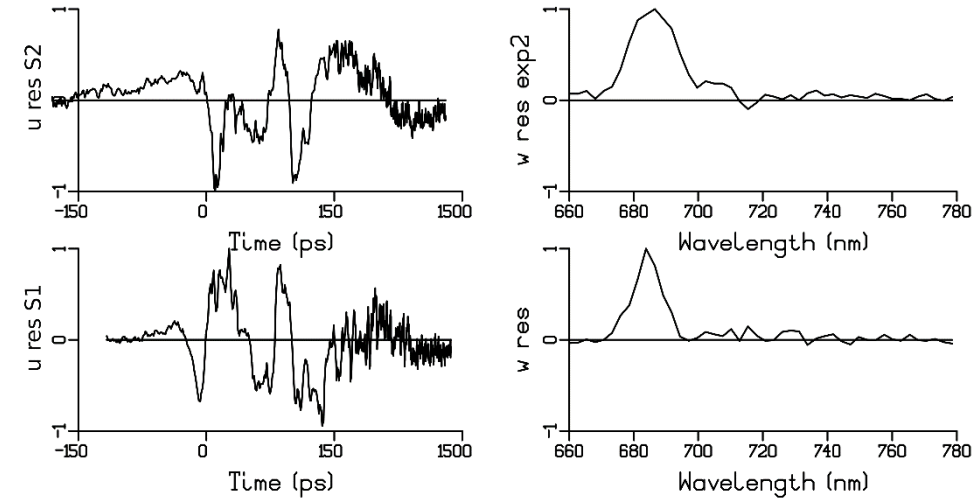


Figure S 12. The first left and right singular vectors resulting from a singular value decomposition of the residual matrix for the two simultaneously analyzed datasets WT S1c & S2c shown in Figure S 11. S1c is depicted in the bottom row, S2c in the top row. Note that the time axis is linear until 150 ps, and logarithmic thereafter.

Although the quality of the fit in Figure S 11 is good, a clear trend in the residual singular vectors in Figure S 12 can be observed corresponding to emission centered around 685 nm (see the right singular vector w res), in particular in S2c, where the left singular vector u res is large and positive from 120-300 ps. Previously this was assigned to a component designated X-685 (Wlodarczyk et al. 2015). No such component was necessary to fit the WT data reported in the present paper and therefore X-685 was not included in the model, but as it was present in the (Wlodarczyk et al. 2015) data, it shows up here in the residual analysis.